Extracellular vesicles within a tumourigenic therapy-induced senescent tumour secretome are able to confer anti-cancer properties.

Matius Robert[1,2,3,4], Rekha Jakhar[1,3,4] and Karen Carmelina Crasta[1,2,3,4#]

Affiliations:

[1]NUS Healthy Longevity Translational Research Programme, Yong Loo Lin School of Medicine, National University of Singapore, Singapore
[2]NUS Centre for Cancer Research, Yong Loo Lin School of Medicine, National University of Singapore, Singapore
[3]Department of Physiology, Yong Loo Lin School of Medicine, National University of Singapore, Singapore
[4]Centre for Healthy Longevity, National University Health System, Singapore

ABSTRACT

Cellular senescence is a fundamental response against chemotherapy to avoid cell death, and the resulting therapy-induced senescent (TIS) cells have been associated with cancer recurrence and therapy resistance via its paracrine activity. The paracrine activity of TIS cells is heavily influenced by the composition and dynamics of the senescence associated secretory phenotype (SASP). The SASP itself is known to be predominantly composed by soluble cytokines, chemokines, and growth factors. The non-soluble fraction of SASP, specifically small extracellular vesicles (sEVs), represents an underappreciated component of SASP and are still poorly characterized. Here we show that the SASP may mediate tumor recurrence and distant metastasis in mice, as well as support invasive and migratory behavior *in-vitro*. Remarkably, while the SASP itself may be pro-tumorigenic, we found that therapy-induced senescent sEVs isolated from the SASP are able to reduce syngeneic tumor growth *in-vivo*. Transcriptomic analysis from therapy-induced sEV recipient mice tissue revealed downregulation of proliferation and mitotic pathways, akin to a senescence-like phenotype, along with upregulation of inflammatory and antigen-presentation pathways. Further characterization revealed that TIS sEVs recipient cells are less invasive and migratory, and that they also exhibit elevated level of reactive oxygen species (ROS), concomitantly with sustained γ-H2AX expression and micronuclei generation. Our results indicate that therapy-induced senescent cancer cell-derived sEVs should be considered as distinct SASP entities.

Although constituting a minority of breast cancers, triple-negative breast cancers (TNBC), the most aggressive breast cancer subtype with poor prognosis, account for disproportionately high metastases, elevated risk of disease relapse and high mortality rates (Yin *et al*, 2020). Since treatment for TNBC is restricted due to lack of specific targets, cytotoxic therapy such as taxane-based chemotherapy, either alone or in combination, remain as mainstay first-line treatment regimen (neoadjuvant or adjuvant) for patients with diagnosis of early-stage, locally advanced and metastatic TNBC (Mustacchi & De Laurentiis, 2015). While most tumours are initially sensitive to treatment, acquired drug resistance can set in, hampering long-term clinical efficacy. Mounting evidence from animal models indicate that cancer therapies can themselves mediate drug resistance via non-cell-autonomous mechanisms, where the altered tumour secretome of drug-sensitive cancer cells confers physiological changes within the tumour microenvironment and growth of these "less-fit" clones (Keklikoglou *et al*, 2019; Obenauf *et al*, 2015; Shi *et al*, 2014). **This highlights the importance of understanding mechanisms by which therapy-induced tumour secretomes exert paracrine influence for potential early detection of disease relapse and better design of treatment regimens for enhanced efficacy.**

An important yet often-overlooked tumour secretome-modulating avenue is therapy-induced senescence (TIS). Cellular senescence, a common therapeutic outcome besides cell death, manifests as a stable cell cycle arrest, conferring tumour suppression. Senescent cells exert their non-cell-autonomous influence on neighbouring cells and the microenvironment via a bioactive secretome consisting of cytokines, chemokines, growth factors and matrix metalloproteinases, termed senescence-associated secretory phenotype (SASP) (Coppe *et al*, 2010; Coppe *et al*, 2008). Soluble SASP factors (sSASP) have been extensively investigated in recent years. In addition to reinforcing senescence in an autocrine manner (Acosta *et al*, 2013; Acosta *et al*, 2008; Kuilman *et al*, 2008), a key role of the sSASP is its paracrine recruitment of immune cells to clear the SASP-producing senescent cells thereby preventing tumour development (Kale *et al*, 2020; Kang *et al*, 2011; Krizhanovsky *et al*, 2008; Xue *et al*, 2007). Interestingly, sSASP paracrine action can also be pro-tumourigenic (Bavik *et al*, 2006; Coppe *et al.*, 2010; Faget *et al*, 2019; Jakhar *et al*, 2018; Wong *et al*, 2018). For instance, sSASP-driven immunosuppressive microenvironments have been shown to engender cancer development and tumour recurrence (Matsuda *et al*, 2023; Ruhland *et al*, 2016).

Although sSASP has been the pivotal focus of SASP function, other entities such as small extracellular vesicles (sEVs), have emerged as important yet under-appreciated component of the senescent secretome (SASP) (Fafian-Labora & O'Loghlen, 2020; Jakhar & Crasta, 2019). sEVs, such as exosomes, are lipid membrane vesicles (size 30nm -150nm) released from tumour cells that serve as vehicles for transfer of signalling molecules (such as nucleic acids, proteins, lipids) from donor to recipient cells (Colombo *et al*, 2014). In this way, they also mediate intercellular communication and modulate the tumour microenvironment, thereby influencing tumour progression and drug resistance (Clancy & D'Souza-Schorey, 2023; Mathieu *et al*, 2019). Indeed,

chemotherapy-elicited EVs have been shown to confer mammary tumour lung metastasis in mice by promoting inflammatory lung endothelial cell activation (Keklikoglou *et al.*, 2019). Similar to sSASP, EVs also possess opposing roles and can elicit tumour suppression. For instance, DNA-containing EVs derived from chemotherapy-treated tumours potentiate anti-tumour immunity via cGAS-STING signalling (Kitai *et al*, 2017). One can extrapolate that the immunomodulatory effect of TIS tumour-derived EVs alone, in the absence of classical SASP factors such as sSASP, hold potential to influence tumour development and therapy resistance. **While it is now established that SASP induction pose prognostic and therapeutic implications in cancer progression and therapy response** [well-reviewed in (Faget *et al.*, 2019; Schmitt *et al*, 2022)]**, the role of senescence-associated EVs in chemoresponse has been largely unexplored (Misawa *et al*, 2020; Wallis *et al*, 2020).** sEV-associated EphA2 secreted from doxorubicin-induced senescent non-transformed cells have been described to promote cancer cell proliferation *in vitro* (Takasugi *et al*, 2017). **However, the impact of EVs derived from tumours rendered senescent by chemotherapies is yet to be characterized.**

In this study, we set out to investigate the role of sEVs derived from paclitaxel-induced senescent TNBCs in tumour development. Unexpectedly, comparative assessment between SASP (whole secretome consisting of sSASP and sEVs) and senescence-associated sEVs alone uncovered distinct tumour phenotypic outcomes.

RESULTS

SASP factors from paclitaxel-induced senescent TNBC cells elicit tumourigenic effects

Our earlier work demonstrated that paclitaxel treatment conferred mitotic slippage-induced senescence and SASP which enhanced tumourigenic phenotypes in xenograft mice harbouring colorectal cancer (Jakhar *et al.*, 2018). As a first step towards understanding tumourigenic potential of the paclitaxel-induced senescent secretome in TNBCs where taxane-based chemotherapy remains standard-of-care, TP53-deficient MDA-MB-231 and TP53-proficient, chromosomally-stable CAL-51 cells were treated with 150 nM Paclitaxel (PTX) for three days to allow mitotically-arrested cells to undergo mitotic slippage and enter therapy-induced senescence (TIS) (**Fig. S1A)** (Brito & Rieder, 2006; Cheng & Crasta, 2017). Indeed, a substantial number of post-slippage MDA-MB-231 cells (~ 67%) collected three days (D3) after PTX-treatment were viable as indicated by the observed tetraploid state, and negligible expression of mitotic markers cyclin B1, phosphorylated histone H3 Ser10, and spindle assembly checkpoint activity (BubR1) (**Fig. S1B-D**). The discernible increase in senescence-associated beta-galactosidase (SA-βgal) activity, enlarged flattened cell morphology, decreased Lamin B1 expression, retinoblastoma protein (Rb) hypo-phosphorylation (Ser780), and increased expression of p21, phosphorylated-p53, DNA damage marker γ-H2AX (**Fig. S1 E, F**), confirmed that these post-slippage cells had entered senescence. Persistence of the senescence-associated markers in cells cultured in fresh media for a further three days (D6), indicated a bona fide

TIS. Similar results were also observed with PTX-treated CAL-51 cells following mitotic slippage **(Fig. S1G-L)**.

To test whether PTX-induced senescent MDA-MB-231 cells could influence tumour growth in xenograft mice, untreated cycling-competent (Cyc) MDA-MB-231 H2B-mCherry cells were subcutaneously injected into immunodeficient NOD/SCID mice either alone or admixed with MDA-MB-231 H2B-GFP cells rendered senescent by prior treatment with PTX (TIS cells) **(Fig. 1A).** As shown in **Fig. 1B**, co-administration of TIS cells significantly accelerated tumour growth, compared to Cyc cells alone, indicating that TIS MDA-MB-231 cells were capable of promoting tumourigenic potential of proliferating cells *in vivo*. This was not due to senescence bypass or escape as the majority of cells dissociated from these tumours expressed H2B-mCherry **(Fig. 1C)**. Importantly, the observation that TIS cells alone did not exhibit tumour growth **(Fig. 1B)** indicated that the accelerated tumour growth was likely attributable to a pro-tumourigenic environment engendered by the co-injected cells. This prompted us to analyse SASP factors (sSASP) since pro-tumourigenic paracrine effects of TIS cells are known to be mediated via their secretome (Bavik *et al.*, 2006; Faget *et al.*, 2019; Jakhar *et al.*, 2018). Luminex-based analysis of conditioned media (CM) prepared from nocodazole (Noc)-induced senescent MDA-MB-231 cells (TIS CM) compared with DMSO-treated cells (Cont CM) **(Day 6; Fig.1D)** revealed upregulation of several cytokines and chemokines known to support tumour cell survival and migration, IL-1α, IL1β, IP-10 (CXCL10), MCP-1 (CCL2), IL-4, GROα (CXCL1), RANTES (CCL5), and platelet derived growth factor AA (PDGF-AA) and PDGF-BB **(Fig. 1E).** To identify gene expression changes in recipient MDA-MB-231 cells following incubation with either No CM (culture media alone), Cont CM or TIS CM (SASP), RNA-sequencing was performed. Data analyses identified 408 genes that were differentially expressed between TIS CM and No CM conditions, and 1064 genes between TIS CM and Cont CM conditions **(Supplementary Table S1).** The most significant REACTOME pathway analysis of the differential expressed genes (DEGs) for TIS CM relative to No CM (TIS vs No CM) were gene sets associated with aberrant upregulation in pathways related to oncogenic signalling, cytokine signalling, and extracellular matrix remodelling, while that for TIS CM relative to Cont CM (TIS CM vs Cont CM) condition were those associated with aberrant upregulation in amino acid metabolism and SLIT-ROBO signalling pathways **(Fig. 1F)**. Gene Set Enrichment Analyses (GSEA) using hallmark gene sets obtained from Molecular Signature Database (MSigDB) displayed high correlation with oncogenic KRAS signalling, epithelial-to-mesenchymal transition (EMT) and cancer-promoting cytokine TNFα signalling for the TIS CM vs No CM gene set, while the TIS CM vs Cont CM gene set showed positive correlation with targets of cell cycle regulator E2F, Type 1 Interferon response (IFN-α) and Type 2 Interferon response IFN-γ, and oxidative phosphorylation **(Fig. 1G),** suggesting a malignancy and pro-inflammatory-related response consistent with a pro-tumourigenic phenotype. Consistent with this, cells incubated with TIS CM compared to No CM showed significantly increased expression of genes implicated in the inflammatory response such as the SASP factors

matrix metalloproteinase-1 (MMP1, top ranked gene), interleukin (IL)-11, programmed death-ligand 1 CD274, cytokine Transforming Growth Factor Beta 1 (TGFβ1), and Wnt ligand WNT5B **(Fig. 1H)**. Interestingly, genes associated with the Wnt signalosome such as FZD1, FZD7, SHH, WNT7B and GATA6 were significantly increased in cells incubated with TIS CM compared to Cont CM **(Fig.1H)**. Indeed, Wnt signalling pathway activation had previously been shown to accompany chemotherapy-induced SASP and EMT gene expression (Basu *et al*, 2012). To assess migratory and invasive capabilities mediated by TIS-induced SASP factors in a paracrine manner, classical wound healing and transwell invasion assays were used. MDA-MB-231 cells incubated with TIS CM promoted wound closure at a rate faster than the Cont CM **(Fig. 1I)**, while an increased number of cells exposed to TIS CM compared with Cont CM invaded the bottom of the filter chamber **(Fig. 1J)** confirming migratory and invasive properties. To assess whether this paracrine pro-tumourigenic effect could be recapitulated *in vivo*, we tested if the secretome of TIS murine TNBC 4T1-12B (4T1) cells could promote tumour growth. To this end, CM derived from nocodazole-treated 4T1 cells confirmed to be senescent **(Supplementary Figure S2A-F),** was incubated with 4T1 cells for nine days and subsequently injected into the mammary gland of syngeneic immunocompetent BALB/C mice. As shown in **Fig.1K (left panel)**, two weeks after orthotopic injection into the mammary fat pad, haematoxylin and eosin (H&E) staining revealed a greater extent of invasive ductal carcinoma when cells exposed to TIS CM were transplanted compared to control CM. This was also confirmed by *in vivo* bioluminescence imaging **(Fig. 1K, right panel)**.

TIS-associated EVs derived from cancer cells impair tumour growth

Given that SASP conferred tumorigenic effects and sEVs are entities inherent within the SASP, we hypothesised that sEVs derived from therapy-induced senescent TNBC cells (TIS sEVs) might also confer tumorigenesis. This expectation was also consistent with a previous report demonstrating that EVs purified from non-transformed senescent cells could confer pro-proliferative effects of several types of cancer cells (Takasugi *et al.*, 2017). To this end, we first sought to assess tumour growth *in vivo* following uptake of sEVs from TIS 4T1 cells. We used sequential ultracentrifugation (UC) followed by size-exclusion chromatography (SEC) to isolate sEVs from 4T1 Cont CM and TIS CM **(Fig. S2G)**. The resulting preparations were highly enriched in sEV as shown by transmission electron microscopy (TEM), Western blot detection of EV markers Alix and TSG101 and nanoparticle tracking analysis (NTA) of sEV concentration **(Fig. S2H-J)**. Consistent with previous reports (Lehmann *et al*, 2008), sEV secretion was found to be more abundant in TIS 4T1 cells compared to control **(Fig. S2J).**

To investigate the function of TIS sEVs during tumor progression, purified CD63-tagged sEVs were administered via six repeated intratumoural injections at 2-day intervals **(Fig. 2A)**. Unexpectedly, EVs purified from TIS TNBCs reduced tumour growth compared to Control EVs (EVs derived from cells treated with DMSO) **(Fig.2B-E)**. Consistent with this, bioinformatic analyses of

RNA sequencing data of TIS EV compared to Control EV as well as Vehicle Control (saline) showed downregulation of oxidative phosphorylation, DNA repair pathway, oncogenic signalling pathways, mitotic pathways **(Fig.2F, G)**. Additionally, GSEA using hallmark gene sets obtained from MSigDB displayed negative correlation with mammary tumour progression and invasion-associated gene sets for TIS EV vs Cont EV **(Fig.2H)**. GSEA using REACTOME gene sets for TIS sEV vs Vehicle showed negative correlation with Wnt pathway and positive correlation with immune response, such as Tcell receptor signalling and antigen-presentation **(Fig.2I).** Tissue staining by immunohistochemistry comparing TIS sEV vs Cont sEV samples demonstrated that TIS sEVs displayed lower proliferative potential (Ki67), robust DNA damage (γH2AX) and p53, higher NF-κB signalling and NKG2D ligand expression, compared to Cont sEV **(Fig. 2J).** TIS EV sample also showed robust SA-β -gal staining, suggesting that EVs may be imparting senescence in murine cancer cells.

To test whether TIS sEVs from human TNBCs were also capable of reducing tumourigenic activity in recipient cells, sEVs were first isolated from MDA-MB-231 cells using the UC+SEC method **(Fig. 3A),** with fractions 7-12 **(Fig.3B)** used in subsequent assays. Western blot detection, NTA and TEM confirmed that the isolated particles were *bona fide* sEVs **(Fig. 3B-D)**, with NTA showing more abundant sEVs in TIS cells. The latter was further confirmed by ELISA and flow cytometric detection of EV-associated marker CD63 **(Fig. S3A, B)**. This was also evident by confocal microscopy with an increased number of TIS cells showing greater extent of co-localisation by immunofluorescence (IF) between CD63 and Rab27a which controls sEV secretion. **(Fig. S3C)**.

To assess cell proliferation and viability in recipient cells following EV uptake, MDA-MB-231 cells incubated with either No sEV, Cont sEV (EVs from cells treated DMSO) and TIS sEV for three days, were used in IF detection of proliferative marker Ki67 and ATP-based cell viability assays. Uptake of sEVs in the recipient cells was confirmed by the PKH67 membrane dye **(Fig. S3D)**. TIS sEV-recipient cells showed reduced cell proliferation and viability compared to Cont EV (**Fig. 3E,F)**. Additionally, the classical wound healing and transwell assays showed decreased migration and invasion respectively in TIS sEV-recipient MDA-MB-231 cells compared to Cont sEV **(Fig. 3G,H)**, indicating that TIS EVs decreased tumourigenic activity in MDA-MB-231 cells. To examine whether p53 status could influence this tumourigenic outcome, we incubated p53 wildtype CAL51 human TNBC cells with MDA-MB-231 cells-derived CM (SASP) and sEVs **(Fig. S4A).** Both wound healing and transwell assays confirmed decreased tumourigenic potential compared to SASP (CM) **(Fig. S4B,C),** showing that alterations in p53 status of TNBCs had null impact. Interestingly, uptake of TIS EVs in the ER+ breast cancer cell line MCF-7 as recipient cell showed negligeable invasion and migration capabilities **(Fig, S4D-F)**.

To extrapolate and visualise this further *in vivo* in real-time, the zebrafish model was used as it is transparent, with cell engraftment and migration readily detectable and quantifiable. MDA-MB-231 cells were incubated with Cont sEV, TIS sEV, or sEV-deficient SASP (CM derived from TIS

MDA-MB-231 cells treated with exosome biogenesis inhibitor GW4869) and injected into zebrafish embryos. As shown in **Fig. 3I, J**, TIS EV-recipient cells showed considerably low migration and invasion compared to SASP. Interestingly, removing EVs from the SASP restored migration and invasive capabilities, strongly indicating that the sEVs represent an intrinsic "anti-tumourigenic" component within the "largely tumourigenic" cancer cell-derived SASP.

TIS-associated EVs induce genomic instability

How do TIS EVs reduce tumorigenic impact of recipient MDA-MB-231 cells? As a first step to answer this, we carried out RNA-sequencing of recipient cells bearing TIS sEVs or Cont sEVs. A decrease in "stemness" and EMT regulators was observed in TIS-recipient cells compared to control **(Fig. 4A, B)**. In addition, RNA-seq analysis showed downregulation of SOD2, a mitochondrial superoxide dismutase pivotal in reactive oxygen species (ROS) release. SOD2 is essential in radical scavenging, which balances the intracellular level of ROS. Western blot detection of NRF2, SOD1 and SOD2 and flow cytometric detection using DCFDA (cell-permeable fluorogenic dye that detects ROS) revealed increased ROS levels in TIS EV-recipient cells compared to control (Fig. 4D). This could be inhibited by the use of N-Acetyl-l-cysteine (NAC, a ROS scavenger) as shown by the increased intracellular GSH/GSSG ratio (Fig. 4E). Is observed ROS elevation accompanied by higher p53 activation and DNA damage? Western blotting showed increased p53 activation and DNA damage levels (γH2AX), with the latter further confirmed by IF detection (Fig. 4G). The results thus far pointed to a role for TIS EVs in inducing genomic instability. To test whether this is so, we examined micronuclei (markers of genomic instability) incidence by IF. Recipient cells bearing TIS EVs showed increased micronuclei frequencies compared to control **(Fig. 4H)**. Notably, all micronuclei observed were acentric, demonstrating that TIS EVs increased chromosome fragmentation that subsequently could be enclosed in micronuclei.

METHODS

Cell culture and construction of stable cell lines. Human cell lines MDA-MB-231, CAL-51, MCF-7, RPE-1, MCF10A, and mouse 4T1 cells were purchased from American Type Culture Collection (ATCC, USA). Cells were cultured in DMEM medium (Gibco, USA) supplemented with 10% fetal bovine serum (FBS; Cytiva), 1% penicillin/streptomycin (P/S; Invitrogen) in a humidified 5% CO_2 incubator at 37°C. The pEGFPC2-CD63 and mCherry-CD81 plasmids (Addgene, USA) were transfected into cells using Lipofectamine 2000 reagent (Invitrogen, USA) according to manufacturer's instructions. G418 (Geneticin, Sigma-Aldrich, USA) was added 48 h post-transfection. After selection for 14 days, stable GFP-CD63 and mCherry-CD81 MDA-MB-231 cell lines were harvested for use. We have confirmed the absence of mycoplasma contamination in our cells.

Therapy-induced senescence induction. Cells were first synchronised by serum starvation-single thymidine method prior to nocodazole or paclitaxel addition. Briefly, cells at 30%-40% confluency were grown in serum-free media for 24 h to reach G0/G1 arrest, washed with DMEM without supplements, and grown in complete media containing 3 mM thymidine (Sigma-Aldrich, USA) for 24 h to reach G1/S arrest. To resume cell proliferation, cells were washed three times with FBS/P/S-free media and grown for further 3h in normal media. Cells were then treated with antimitotic drug Nocodazole (Noc, 100 ng/ml; Sigma-Aldrich, USA) or Paclitaxel (PTX, 150 nM; Sigma-Aldrich, USA) for 72 h to achieve therapy-induced senescence (TIS) state.

Viability assay. Cell viability and proliferation was assayed using CellTiter 96 Aqueous One Solution Reagent (Promega, USA) according to manufacturer's instructions.

Senescence-associated β-galactosidase (SA-β-gal) staining. SA-β-Gal activity was measured using the SA-β-gal staining kit (Cell Signaling Technology, USA) following manufacturer's protocol. Number of blue cells (senescent) relative to the total cell number was counted in two to four different optic fields using EVOS microscope 40X objective lens (Thermo Fisher Scientific, USA). At least 200 cells were counted per sample.

Total RNA extraction, cDNA synthesis and qRT-PCR. Total RNA was isolated using RNeasy Plus kit (Qiagen, USA). RNA quality and concentration were determined using NanoDrop 2000 system (Thermo Fisher Scientific, USA). Reverse transcription of RNA to cDNA was performed using the iScript cDNA synthesis kit (Bio-rad Laboratories, USA). cDNA was mixed with SYBR Select Master Mix for CFX (Applied Biosystems, USA) and relevant primers (Integrated DNA Technologies, USA). Quantitative real-time PCR (qRT-PCR) reaction was carried out with Step-One Plus system (Thermo Fisher Scientfic, USA).

Flow cytometry. Cells were fixed overnight with ice-cold 70% ethanol (Sigma-Aldrich, USA). For phospho-histone-H3/propidium iodide analysis, fixed cells were washed twice in PBS with 0.5% BSA prior to incubation with 1:500 dilution of phospho-histone H3 antibody conjugated with Alexa Fluor 488 (Cell Signaling Techonology, USA) for 1 h in the dark at room temperature. The samples were then washed in 0.5% BSA in PBS and incubated with 250 µg/ml RNase A (Sigma-Aldrich, USA) and 10 µg/ml propidium iodide (PI, Sigma-Aldrich, USA) at 37°C for 30 min before analysis. FACS analyses were performed with BD Accuri C6 Flow cytometer (BD Biosciences, USA) using two-parameter scanning; FL1-H (FITC) versus FL2-A (PI) and data analysed using FlowJo software (BD Biosciences, USA).

Immunoblotting. For total protein isolation, cells were lysed in RIPA buffer (Pierce, USA) containing protease/phosphatase inhibitor cocktail (Thermo Fisher Scientific, USA). Cytoplasmic and nuclear portion of protein were extracted by NE-PER nuclear and cytoplasmic extraction reagents (Thermo Fisher Scientific, USA). Protein concentration was measured using the Bradford assay (Bio-Rad Laboratories). An appropriate volume of Laemmli sample buffer was added to equal amounts of total protein followed by boiling for 5 min. Samples were subjected to SDS–PAGE electrophoresis before transfer to nitrocellulose membrane (Bio-Rad Laboratories, USA). After blocking for 1 h in 5% skim milk/PBST, cells were incubated overnight at 4°C in primary antibody diluted in 3% skim milk/PBST. Membranes were then washed three times with PBST and incubated with HRP-conjugated secondary antibody diluted in 3% skim milk/PBST. Signal was detected using enhanced chemiluminescence (ECL) (GE Healthcare Life Sciences, USA) and ChemiDoc imaging system (Bio-Rad Laboratories, USA).

Immunofluorescence. Cells grown on coverslips were fixed in PBS/4% paraformaldehyde (PFA) for 10 min at room temperature. Cells were then washed twice with PBS, permeabilised with PBS containing 0.1% Triton X-100 (PBST) and incubated in blocking buffer (PBST/10% FBS/1% BSA) for 30 min. Cells were then incubated in blocking buffer containing primary antibody overnight at 4°C. Following three washes with PBS containing 0.1% Triton X-100 (PBST), cells were incubated in blocking buffer containing secondary antibody for 2 h at room temperature. Nuclei were stained with Hoechst stain for 10 min at room temperature. Images were captured using Nikon Inverted Microscope Eclipse Ti-E (Nikon) and Orca ER CCD camera (Hamamatsu Photonics).

Conditioned media preparation. 72h after drug addition, TIS MDA-MB-231 cells were grown in reduced serum media DMEM/0.5% FBS/1% P/S for further three days. Cell culture medium was collected and centrifuged at 5000×g and the supernatant filtered with 0.22 μm pore filter (Pall Corporation, USA). This was mixed with media containing 40% FBS in a proportion of 3:1 to generate conditioned media (CM) containing 10% FBS.

Chemokine and cytokine analyses. CM was collected from TIS MDA-MB-231 cells for chemokine and cytokine analyses using a Milliplex MAP human cytokine/chemokine magnetic bead panel (Merck Millipore) according to the manufacturer's protocol.

sEV isolation from conditioned media. For sEV isolation using ultracentrifugation protocol, CM was prepared after drug or DMSO treatment by incubating cells in growth media containing 5% exosome-depleted FBS (Thermo Fisher Scientific, USA) for 72 h. CM was then collected and centrifuged at 500×g for 10 min, 2,000×g for 30 min, and 15,000×g for 30 min at 4°C to remove cells and large debris. The supernatant was then filtered using 0.22 μm pore filter (Pall Corporation, USA),

and EVs pelleted at 120,000×g for 2 h at 4°C. The EV pellet was washed with PBS and pelleted again by centrifugation at 100,000×g for 1 h at 4°C. Isolated EVs were further dissolved in 0.5 ml of PBS and purified using SEC-qEV2/35 nm columns (Izon Science, New Zealand) for size-exclusion chromatography (SEC). After rinsing the qEV columns with PBS, 0.5 ml of EV sample were applied on top of the column, equilibrated, and eluted with PBS in 30 fractions (0.5 ml/fractions). Two sets of four EV-rich fractions (7–12 and 16-22) were pooled and concentrated using Amicon Ultra-4 10 kDa centrifugal filter device (Merck Millipore, USA). Alternatively, sEV isolation was performed using the Total Exosome Isolation Reagent (from cell culture media) kit (Invitrogen, USA) according to manufacturer's protocol. Briefly, CM was incubated with kit reagents at 4°C, and precipitated sEVs recovered by centrifugation at 10,000xg for 60 min.

sEV detection and quantification. For Nanoparticle Tracking Analysis (NTA), sEVs were quantified based on size distribution using NanoSight NS300 (Malvern Instruments, UK). For data acquisition, approximately 10 µl of EV suspension diluted in final volume of 1 ml, was loaded into the sample chamber of the NanoSight using a sterile syringe. Samples were captured at 20-25°C with camera level of 13 and gain of 250–300 over 60 s in triplicates. For data analysis, a detection threshold of 3 and Blur/track length/expected size set at Auto were used. Data were analysed with the Nanosight NTA software version 3.1 (Malvern Panalytical, UK). Alternatively, EVs were quantified with the ExoELISA Complete Kit (CD63 Detection, System Biosciences, USA) according to manufacturer's instruction. For detection and quantitation of surface CD63 by flow cytometry, SEC fractions were incubated overnight with anti-CD63 magnetic beads (Thermo Fischer Scientific, USA) with continuous rotation at 4 °C. This was followed by flow cytometric detection after staining of bead-bound sEVs with fluorescent anti-CD63 phycoerythrin (PE) (Sigma-Aldrich, USA).

Transmission electron microscopy. Aliquots from pooled EV-rich SEC fractions (F7-12) were deposited onto formvar-coated 400 mesh copper grids for 7 min at room temperature and thereafter stained with 2% uranyl acetate (Electron Microscopy Services, USA). Grids were imaged using transmission electron microscope Tecnai T12 (Thermo Fisher Scientific, USA).

Visualisation of EV uptake. MDA-MB-231-derived sEVs were labelled using the PKH67 Green Fluorescent Cell Linker kit (for general cell membrane labelling, Sigma-Aldrich, USA) according to manufacturer's protocol. Cells were also stably transfected with GFP-CD63 and mCherry-CD81 plasmids (Addgene, USA) for exosomal tracking. Recipient cells were incubated with either PKH67 dye-labelled or fluorescent-labelled sEVs for 2-3 days in media supplemented with 5% exosome-depleted FBS (Gibco, USA). Cells were imaged with time-lapse microscopy or washed with PBS, fixed in 4% PFA for 15 min and examined under Nikon Eclipse Ti microscope for immunofluorescence.

Tandem mass tag labelling and data analysis. Protein was isolated from purified EVs using Total Exosome RNA & Protein Isolation Kit (Invitrogen, Thermo Fisher Scientific) following manufacturer's instructions. 100 µg protein of the EV lysate in 8 M urea was alkylated with dithiothreitol (DTT) and iodoacetamide (IAA), diluted with seven volumes of PBS and digested with Trypsin/Lys-C for proteolytic digestion. The reaction was quenched by heating at 60 °C. Digested proteins were desalted, dried and dissolved in 200 mM triethylammonium bicarbonate buffer (pH, 8.5). Tandem Mass Tagging (TMT) labelling was performed using Tandem Mass Tag Reagents kit (Thermo Fisher Scientific, USA) following manufacturer's protocol. Different TMT labels were used to label different groups: TMT-126, 127, and 128 were used for cont-sEV group; TMT-129, 130, and 131 for TIS-sEV group. After labelling, samples were pooled, dried and dissolved in 0.1% trifluoroacetic acid (TFA). The samples were then desalted, dried and dissolved in 100 µL of 0.1% TFA. ExoCarta (web-based compendium of exosomal cargo) were used to identify exosomal protein cargo, with the top 100 sEV proteins then further analysed using DAVID software. Proteins identified were also subjected to pathway enrichment analyses and visualization using R v4.1.2. Gene Ontology (GO) enrichment analysis was performed by clusterProfiler v4.2.2, while Reactome enrichment analysis was by ReactomePA v1.38.0. For visualization, enrichment analyses and volcano plot were constructed using enrichplot v3.15 and EnhancedVolcano v1.14.0 respectively.

RNA sequencing analyses. Isolated RNA samples were sent to NovogeneAIT Genomics Pte Ltd (Singapore) for sequencing. Briefly, raw reads of fastq format were firstly processed through fastp software to obtain clean reads by removing reads containing adapter, poly-N and low-quality reads from raw reads. RNA-seq reads were then aligned to the human genome using Hisat2 v2.0.5, and featureCounts v1.5.0-p3 was used to count reads numbers mapped to each gene. Differential expression analysis was performed using DESeq2. The resulting p-values were adjusted using the Benjamini and Hochberg's approach for controlling the false discovery rate. Genes with an adjusted p-value (padj) ≤ 0.05 found by DESeq2 were assigned as differentially expressed unless otherwise stated. Resulting differentially expressed gene list was used for downstream enrichment analyses. Gene Ontology (GO) enrichment analysis was performed by clusterProfiler v4.2.2, while Reactome enrichment analysis by ReactomePA v1.38.0. For enrichment visualization, enrichment analyses and volcano plot were constructed using enrichplot v3.15 and EnhancedVolcano v1.14.0 respectively. Lastly, gene set enrichment analysis (GSEA) was performed using fgsea v4.2.

Cellular reactive oxygen species (ROS) measurement. Cells incubated with sEV for 72h were trypsinised and washed twice with PBS. After washing, cells were stained with 20 µM of 2',7'–dichlorofluorescin diacetate (DCFDA) (ab113851) (Abcam, USA) for 30 min at 37 °C and

analysed on an Accuri C6 flow cytometer (BD Biosciences, USA) under FL-1 channel. Data were analysed using FlowJo software.

GSH/GSSG ratio measurement. GSH/GSSG ratios were measured using GSH/GSSG-Glo™ Assay (Promega) according to the manufacturer's protocol. Briefly, cells were lysed using Total Glutathione Lysis Reagent and Oxidized Glutathione Lysis Reagent. After lysis, Luciferin Generation Reagent was added unto the wells and plate was incubated for 30 minutes at room temperature. Subsequently, Luciferin Detection Reagent was added unto the wells, followed 15 minutes incubation and luminescence measurement.

Wound healing assay to assess migration. Cells were seeded in 6-well plates to reach confluency. The confluent monolayer was scratched with a 200 µl pipette tip to generate a wound and incubated for 72 h with CM or sEV-containing media ($2x10^9$ particles/ml). Phase-contrast images were captured at 24 h, 48 h, and 72 h timepoints under 10X objective lens and analysed using ImageJ.

Transwell assay to assess invasion. Cells were incubated with CM or media containing sEV ($2x10^9$ particles/ml) for three days. Cells were then trypsinized, resuspended in CM or sEV-containing media, seeded onto transwell inserts (8 µm pore size) pre-coated with Matrigel (BD Biosciences, USA), with 20% FBS added to the lower chamber and further incubated for 24h. Non-invasive cells were removed from the upper surface of the inserts and invasive cells on the lower surface were fixed with PFA, stained with crystal violet and observed under 10X objective lens. The number of invaded cells in six to nine random fields were counted per condition.

Animal work

Quantification of cellular migration and metastasis in zebrafish (ZgraftTM). The Zebrafish Research Facility in Acenzia is certified via Ontario Ministry of Agriculture, Food and Rural Affairs (OMAFRA). All protocols used were monitored by the Animal Health and Welfare Branch, OMAFRA. Fish in the facility were housed and maintained using Tecniplast's ZebTec system with a controlled day-night (14 h light/10 h dark) light cycle. Embryos obtained from natural spawnings and developmental stages are reported as hours post-fertilization (hpf) at 28.5°C. sEVs were isolated from drug-treated senescent MDA-MB-231 cells. MDA-MB-231 cells were incubated with the sEVs at a concentration of $2x10^{10}$ particles/ml, or with conditioned media (SASP or sEV depleted-SASP) two days before injection. For collecting conditioned media with sEV-depleted-SASP, MDA-MB-231 cells after treatment with 15 µM N-Smase inhibitor GW4869 (Sigma-Aldrich, USA) for 72h, were grown in reduced serum media DMEM/0.5% FBS/1% P/S for further three days. Conditioned media was collected and processed as mentioned before. Xenotransplanted MDA-MB-231 cells were visualised in the zebrafish embryos by red fluorescence by staining with Vybrant DiI (Life

Technologies, USA). Cells from each treatment were detached at 80% confluency using Trypsin-EDTA solution (Sigma-Aldrich, USA). Cells were further incubated for 45 min at 37°C in serum-free culture media containing DiI at a concentration of 5 μl dye per million cells. Cells were then washed twice and re-suspended in serum-free media for injection. Zebrafish embryos at 48 hpf were then dechorionated when required and anesthetised with tricaine (Sigma-Aldrich, USA). Using Nanoject II (Drummond Scientific, USA) injector, approximately 100 cells were injected into the yolk of each embryo. Embryos were then incubated for 2 h at 32°C and checked for successful injection. Embryos with fluorescent cells outside the yolk sac were excluded from further experimentation and analysis. Accurately-injected embryos were further incubated at 32°C in a fresh fish tank system water for 48 h and imaged. Embryos were anesthetised on a microscope slide at 48 h post-injection and imaged using Leica M165 LC. Images were gathered, aligned to a specific orientation and analysed by ImageJ software to determine metastatic tumour foci position relative to injection site (0,0 on graph). Tumour foci observed in all tested larvae, in each treatment group (presented as n on the graph), were presented as scatter plots. All foci in one larva were represented by a single colour. For consistent quantitative comparison of differentially treated cells, Invasion Index measured the ability of cells to invade, and Migration Index measured the ability of cells to migrate. These were calculated as follows: Invasion index = Number of metastases formed per 100 cells injected. Migration index = Distance travelled by metastases as percent of the maximum distance cells can migrate within the fish.

Mice xenograft experiments

All animal experiments were conducted in accordance with the National Advisory Committee for Laboratory Animal Research (NACLAR) Guidelines and approved by the National University of Singapore (NUS) Institutional Animal Care and Use Committee (IACUC) under Protocol No. R18-0635. BALB/c mice were purchased from InVivos, Singapore. Mice were kept on a 12-h light/dark cycle with food and water provided *ad libitum* and maintained under pathogen-free conditions in the Animal Housing Unit, Comparative Medicine Department at the National University of Singapore.

Immunocompromised (NOD/SCID) Balb/c female mice were transplanted subcutaneously into the right flank with $2.5x10^6$ untreated cycling-competent (cyc) MDA-MB-231 cells alone, $2.5x10^6$ cyc MDA-MB-231 cells and $0.5x10^6$ cells paclitaxel-induced senescent MDA-MB-231 cells, or $2.5x10^6$ cells paclitaxel-induced senescent MDA-MB-231 cells alone.

NOD/SCID female mice 6–8 weeks of age were injected subcutaneously (sc) under anesthesia with 2.5 × 106 MDA-MB-231 cells on the right flank. When tumors reached a volume of about 100 mm3 , mice were randomized into two groups of five and six animals, and received a total of 7 ip injections of 100 μl saline containing 100 μg either Andes-1537 (group of 5) or ASO-C (group of 6) on days 12, 14, 16, 19, 21, 23, and 26 post-cell inoculation, in a blinded fashion. Tumor growth was monitored

with a caliper and tumor volumes were calculated following the formula: tumor volume = length × width2 × 0.5236. Mice were sacrificed under anesthesia on day 27 after cell injection.

Tumour implantation, sEV challenge and bioluminescence imaging of 4T1 tumour.
Fifteen mice were randomised into three groups (saline, DMSO control sEVs, and TIS sEVs, 5 mice per group) 50 μl of sterile PBS containing 1×10^5 4T1-12b cells were injected into the mammary fat pad of BALB/c mice. Upon reaching a tumour size of approximately 100mm^3, 50 μl of saline, control sEVs or TIS sEVs generated from mouse breast cancer 4T1 cells at a concentration of 4×10^9 particles/50 μl, were injected intratumourally every other day for 6 injections. Mice were weighted prior to, during and post-injection. Tumours were localized and quantitated using bioluminescence-based Xenogen IVIS Spectrum Imaging System (PerkinElmer, USA). Briefly, mice were injected with 150 μL of VivoGlo Luciferin (150 mg/kg) (Promega, USA) intraperitoneally prior to imaging and put under isoflurane anaesthesia during imaging. Tumour volumes were measured manually using a digital calliper and volume calculated as follows: V (mm^3) = length (mm) × width (mm) × width (mm)/2). Mice were euthanized either at the end of the study or earlier if they displayed significant weight loss, signs of distress, or palpable tumours ≥2.0 cm in diameter. Tumours were excised and used for downstream molecular analyses.

Mice tumour-associated immune cell characterisation. Cells were stained with flexible viability dye eFluor 506 (myeloid panel-1:1000) or near IR (lymphoid panel-1:100) (Thermo Fisher Scientific, USA). Cells were subsequently stained with the following cocktail: CD45-AF700, CD 11b-FIC, CD86-APC, CD206-PE/Cy7, MHC Class II- APC eFlour 780, LY-6G-PE, F4/80-PB, CD11c-PE eFluor 610 (Myeloid Panel) or F4/80-PE/Cy, CD278-AF647, CD8a-BV421, CD45-BV711, CD279-PE-CF594, CD3e-BUV395, CD4-AF488, CD25-PE (Lymphoid panel). Cells were analysed on a BD LSRFortessa X-20 (BD Biosciences, USA) with data analysed using FlowJo software.

Immunohistochemistry of mice tissues. Harvested mice tissues were stored in 4% PFA overnight followed by sequential dehydration with 15% ethanol (overnight) and 30% ethanol (overnight). Tissues were then mounted on mounting blocks made from Tissue-Tek O.C.T. (Sakura) at -20C, before being sliced by cryostat at 10 uM thickness with a cryostat (Leica Microsystems CM3050S). Slices were picked up onto cover slides and rinsed by deionized water briefly followed by haematoxylin staining for 10 min and eosin counterstain for 20 seconds. Slices were then washed with 95% ethanol and xylene before being mounted in xylene-based mounting media on the coverslips. After the mice tissues were dehydrated and sliced with cryostat as per protocol above, slices were picked up on coverslips and briefly rinsed with PBS. Slices were then blocked with blocking buffer (PBS, 5% Normal Donkey Serum, 0.3% Triton-X) at 4 °C for 1 h, and subsequently incubated with primary antibodies overnight. Slides were then washed three times with PBST at 4 °C for 10 min, and

incubated with blocking buffer containing secondary antibodies (1:200) at room temperature for 2 h. This was followed by three PBST washes and DAPI counterstain. Slices were then mounted onto slides with mounting media.

Quantification and statistical analysis. All experiments were performed independently at least three times. Statistical analyses were performed using Prism 9 software (GraphPad), and statistical information pertaining to the number of replicates and significance can be found in Figure Legends. Significance levels for comparisons between two groups were determined with two-tailed Student t-test, and for comparisons of more than two groups were determined with one-way analysis of variance (ANOVA). Data were plotted as mean ± SD.

Data availability

The RNA-seq dataset generated and analysed in the study is available in the NCBI GEO repository with accession code GSE236953, GSE237710, and GSE238165. DEGs identified in CM incubated and sEVs incubated MDA-MB-231 cells can be found in Supplementary Table S1 and S3 respectively, while DEGs identified in orthotopic breast tumour mice injected with sEVs can be found in Supplementary Table S2.

CONCLUSION

Therapy-induced senescent-cancer cell-derived small extracellular vesicles can impart anti-tumourigenic paracrine effects.

Figure 1

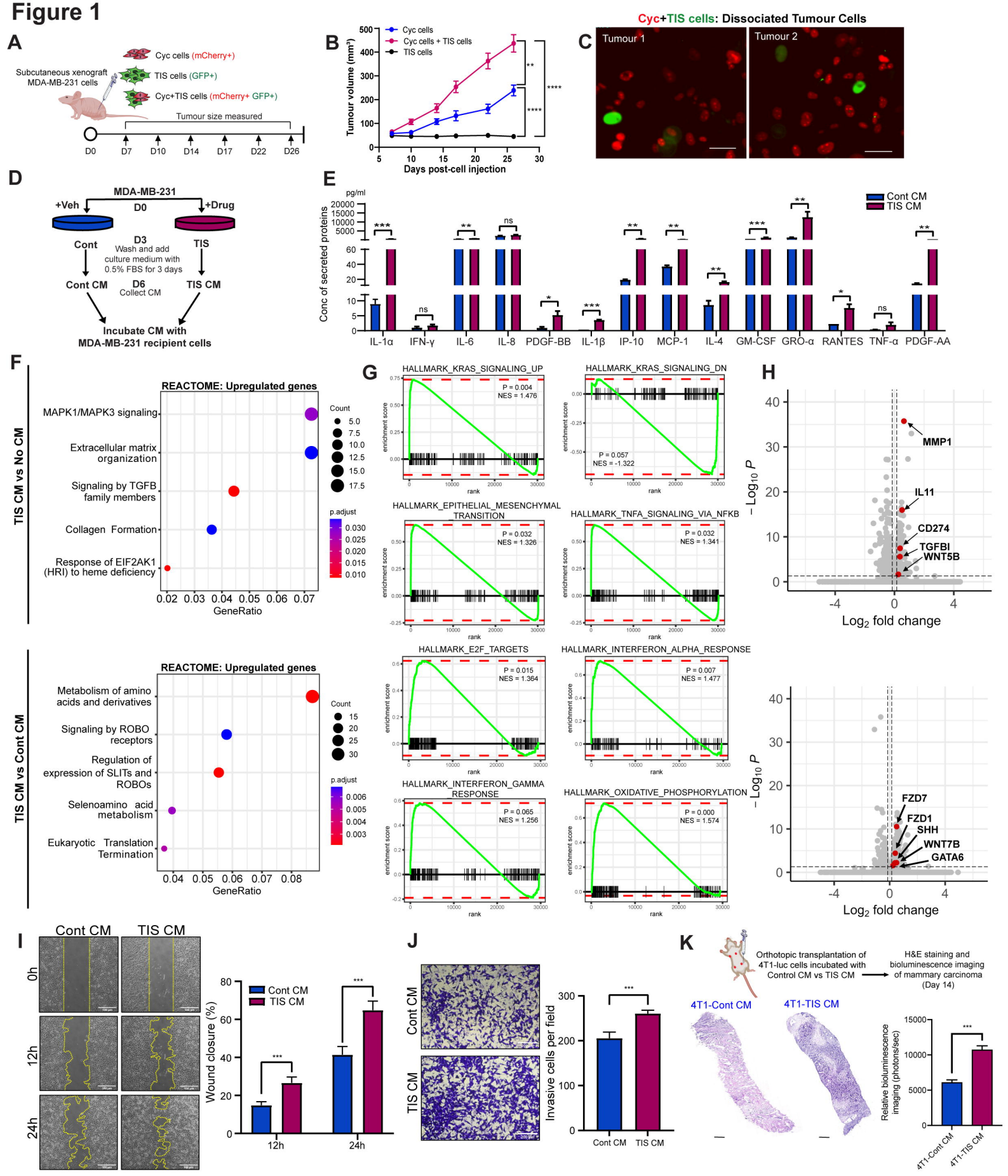

Figure 1. Paclitaxel-induced senescent MDA-MB-231 human breast cancer cell-derived SASP accelerates tumourigenic effects in a paracrine manner. (**A**) Experimental scheme of subcutaneous injection into flank region of NOD/SCID mice of (i) non-senescent cycling-competent (Cyc) MDA-MB-231-mCherry + cells (ii) cyc mCherry+cells and TIS GFP+ cells (ii) TIS GFP+ cells alone. (**B**) Tumour volume (mm³) was measured at indicated timing (n = 8-10 mice per group). (**C**) Representative image for dissociated tumour cells with cyc mCherry+ and TIS GFP+ cells. (**D**) Experimental scheme for TIS induction for conditioned media (CM) collection from synchronised MDA-MB-231 cells treated with 100 ng/ml of nocodazole (Noc) or DMSO control; D:Day. (**E**) Luminex cytokine analysis of Cont CM and TIS CM (Day 6). (**F**) REACTOME enrichment analysis of differentially expressed genes (DEGs) in MDA-MB-231 recipient cells from (top) TIS CM vs No CM and (bottom) TIS CM vs Cont CM conditions showing top five upregulated pathways. (**G**) Gene set enrichment analysis (GSEA) of (top) TIS CM vs No CM and (bottom) TIS CM vs Cont CM expression datasets using hallmark gene sets obtained from Molecular Signature Database (MSigDB). (**H**) (top)Volcano plot of DEGs in cells incubated with TIS CM vs No CM, vertical dotted line denotes $pLog_2FC \leq -0.15$; $Log_2FC \geq 0.15$, horizontal dotted line denotes Padj ≤ 0.05. (bottom) Volcano plot of DEGs in cells incubated with TIS CM vs Cont CM, vertical dotted line denotes $Log_2FC \leq -0.15$; $Log_2FC \geq 0.15$, horizontal dotted line denotes Padj ≤ 0.05. (**I**) Representative images and quantification of wound closure after incubation with Cont CM or TIS CM. Scale bar: 100 µm. (**J**) Representative images and quantification of recipient cells that invaded transwell after 72h incubation with Cont CM or TIS CM. Scale bar 200 µm. Data are mean ± s.d. of 3 independent experiments. *p < 0.05, **p < 0.01, ***p < 0.001, ****p < 0.0001, and n.s. non significance by Student's *t*-test. (**K**) Mice were orthotopically injected with 4T1-luc cells previously exposed to either Cont CM or TIS CM for nine days, n=10 mice per condition. (Left panel) Representive imagesof haemotoxylin and eosin (H&E) staining showing extent of invasive ductal carcinoma at day 14 post-transplantation. (Scale bar, 1mm). (Right Panel) Quantification of bioluminescence activity 14 days post-transplantation, relative to activity recorded on day 1 after cell transplantation (n=10 per group).

Figure 2

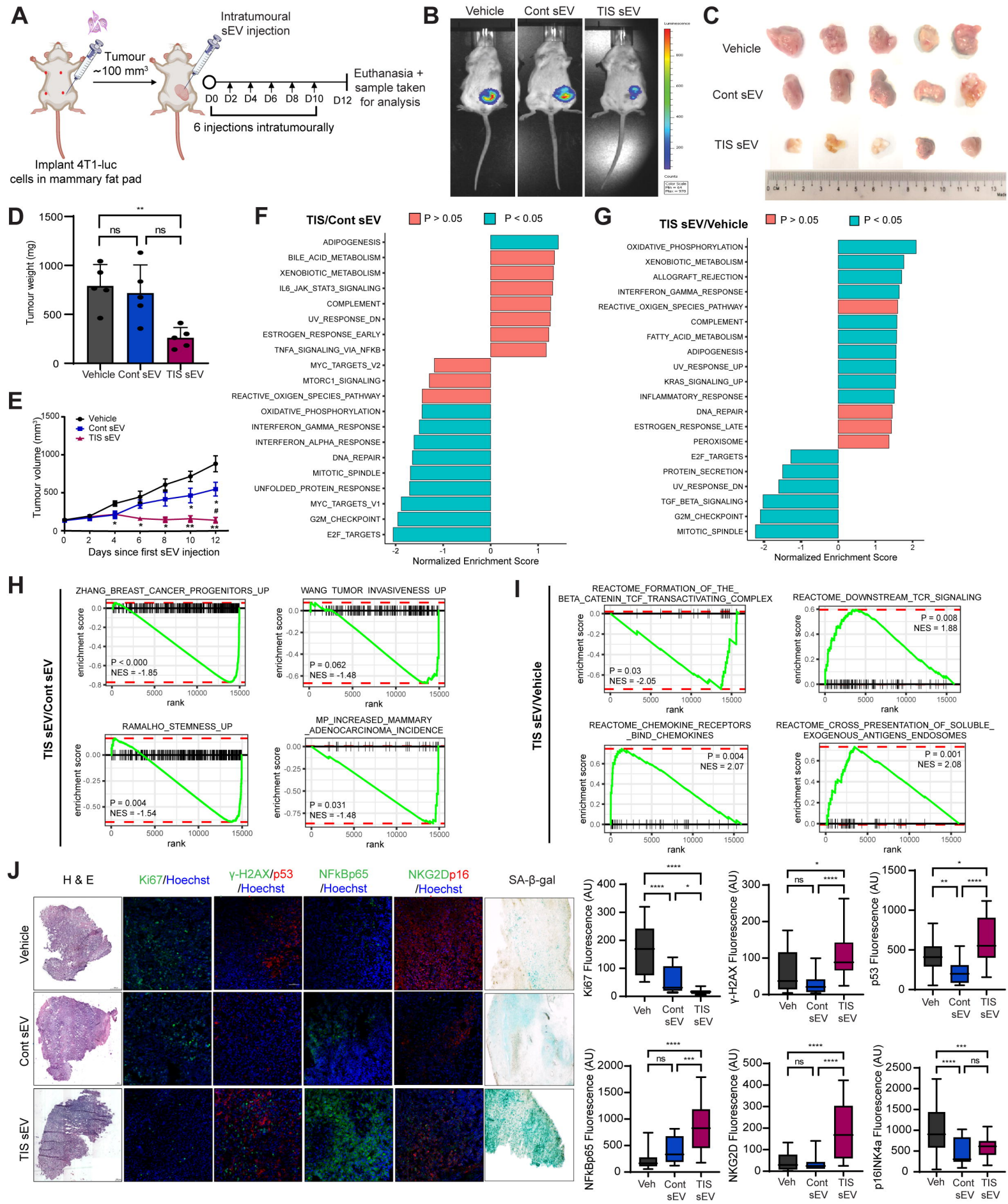

Figure 2. TIS derived sEVs from 4T1 murine cancer cells reduces syngeneic tumour growth *in vivo*. (**A**) Schematic for *in vivo* sEV uptake by mouse. BALB/c mice bearing 4T1-luc tumours in their mammary fat pads were injected intratumourally with 4 × 10^9 4T1 sEV dissolved in 50 µl PBS. (**B**) Bioluminescence imaging for mice 12 days post-injection. (**C**) Representative images of xenograft tumours harvested from mice after 12 days of indicated treatment. (**D**) Tumour weights measured at the end of the experiment and compared. Dots represent individual tumour weight. (**E**) Tumour volumes were calculated by LxWxW/2 and compared. (**F**) HALLMARK GSEA of TIS vs Cont sEV expression dataset. (**G**) HALLMARK GSEA of TIS sEV vs Vehicle control (saline) expression dataset. (**H**) GSEA of TIS vs Cont sEV expression dataset using stemness and invasion related gene sets obtained from MSigDB. (**I**) GSEA of TIS vs Cont sEV expression dataset using REACTOME gene sets. (**J**) H&E staining, immunofluorescence staining (against indicated antibodies) and SA-β-gal staining for tumour tissue (left). Quantification of relative fluorescence intensity in tumour tissue (right). Data shown are mean ± SEM (n = 5 mice per group). *p < 0.05, **p < 0.01, ***p < 0.001, ****p < 0.0001, #p<0.05 vs Cont sEV, and n.s. non significance by Student's t-test.

Figure 3

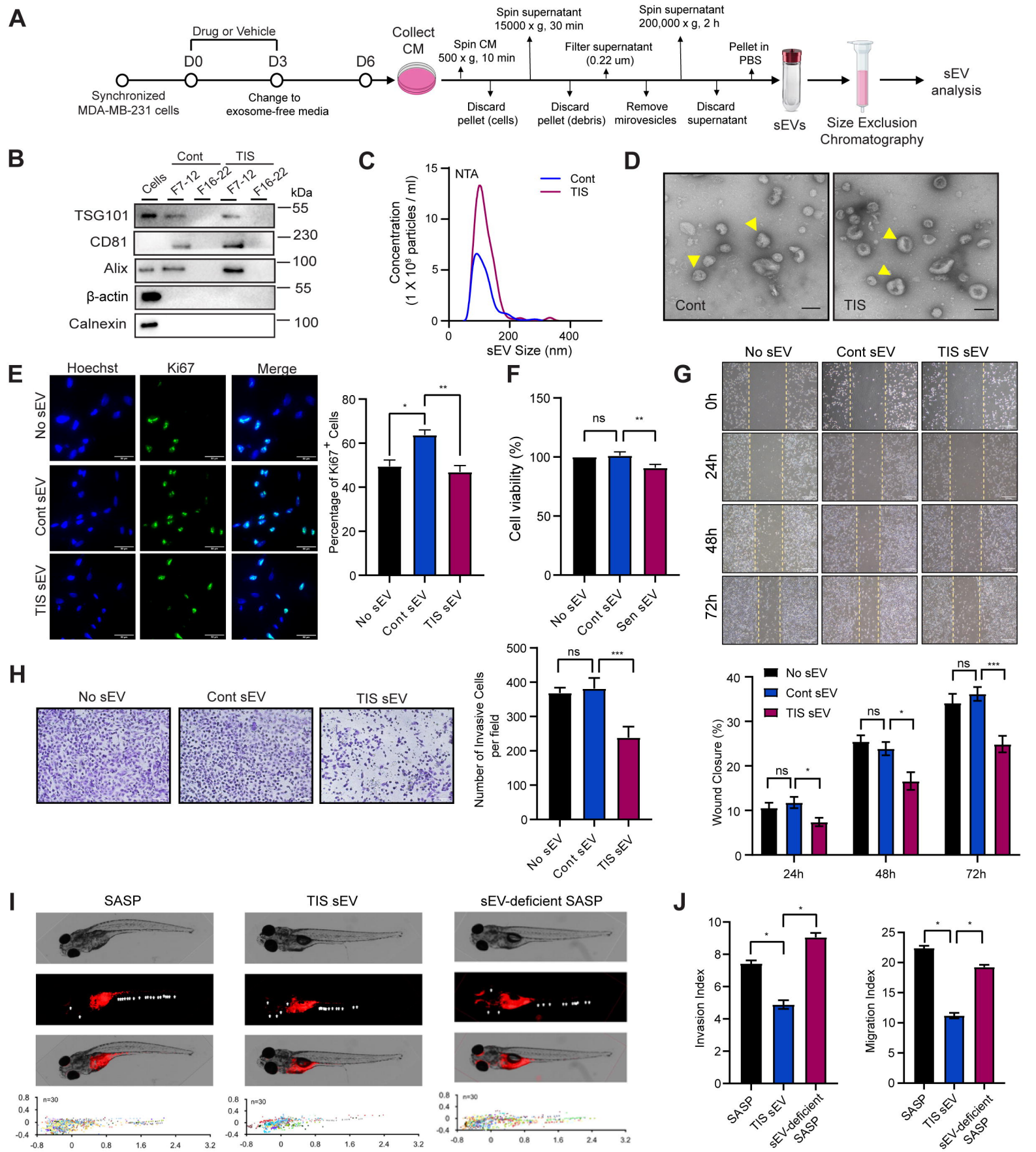

Figure 3. sEVs from TIS MDA-MB-231 cells ameliorate invasive and migratory capacity. (**A**) Schematic for sEV isolation from Cont and TIS MDA-MB-231 breast cancer cells using differential ultracentrifugation (UC) and subsequent purification by size exclusion chromatography (SEC). **(B)** Immunoblot detection of eluted EV fractions (SEC fraction found to be 7-12), eluted protein fraction (SEC fraction 16-22), cell lysate for EV markers (Alix, CD81, TSG101) and negative controls (β-actin, calnexin). (**C**) sEVs were quantified using nanoparticle tracking analysis (NTA). Representative concentration vs size plot for Cont and TIS-derived sEVs. (**D**) Yellow arrows indicate representative transmission electron microscopy (TEM) images of sEVs isolated from Cont and TIS cells. Scale bar: 100 µm. (**E**) Representative immunofluoresence images and quantification of Ki67 positive MDA-MB-231 cells after 72h incubation with No sEV, Cont sEV, and TIS sEV. Scale bar: 50 µm. (**F**) Cell viabillity quantification of MDA-MB-231 cells after 72h incubation with No sEV, Cont sEV, and TIS sEV. (**G**) Representative images and quantification of wound closure on recipient MDA-MB-231 cells after 72h incubation with No sEV, Cont sEV, and TIS sEV. Scale bar: 100 µm. (**H**) Representative images and quantification of invasive recipient MDA-MB-231 cells after 72h incubation with No sEV, Cont sEV, and TIS sEV. Scale bar: 200 µm. (**I**) Representative zebrafish to track migration and invasion. MDA-MB-231 cells were incubated with SASP, TIS sEV, or sEV-deficient SASP, followed by injection to zebrafish embryo. Injected MDA-MB-231 cells in zebrafish stained with Vybrant Dil. Tumour foci were presented as scatterplot, while 'n' denotes the number of injected embryos from three biological replicates. (**J**) Quantification of metastatic ability of injected MDA-MB-231 cells by invasion index (left) and migration index measurement (right). Data are mean ± s.d. of 3 independent experiments. *p < 0.05, **p < 0.01, ***p < 0.001 and n.s. non significance by Student's t-test.

FIGURE 4

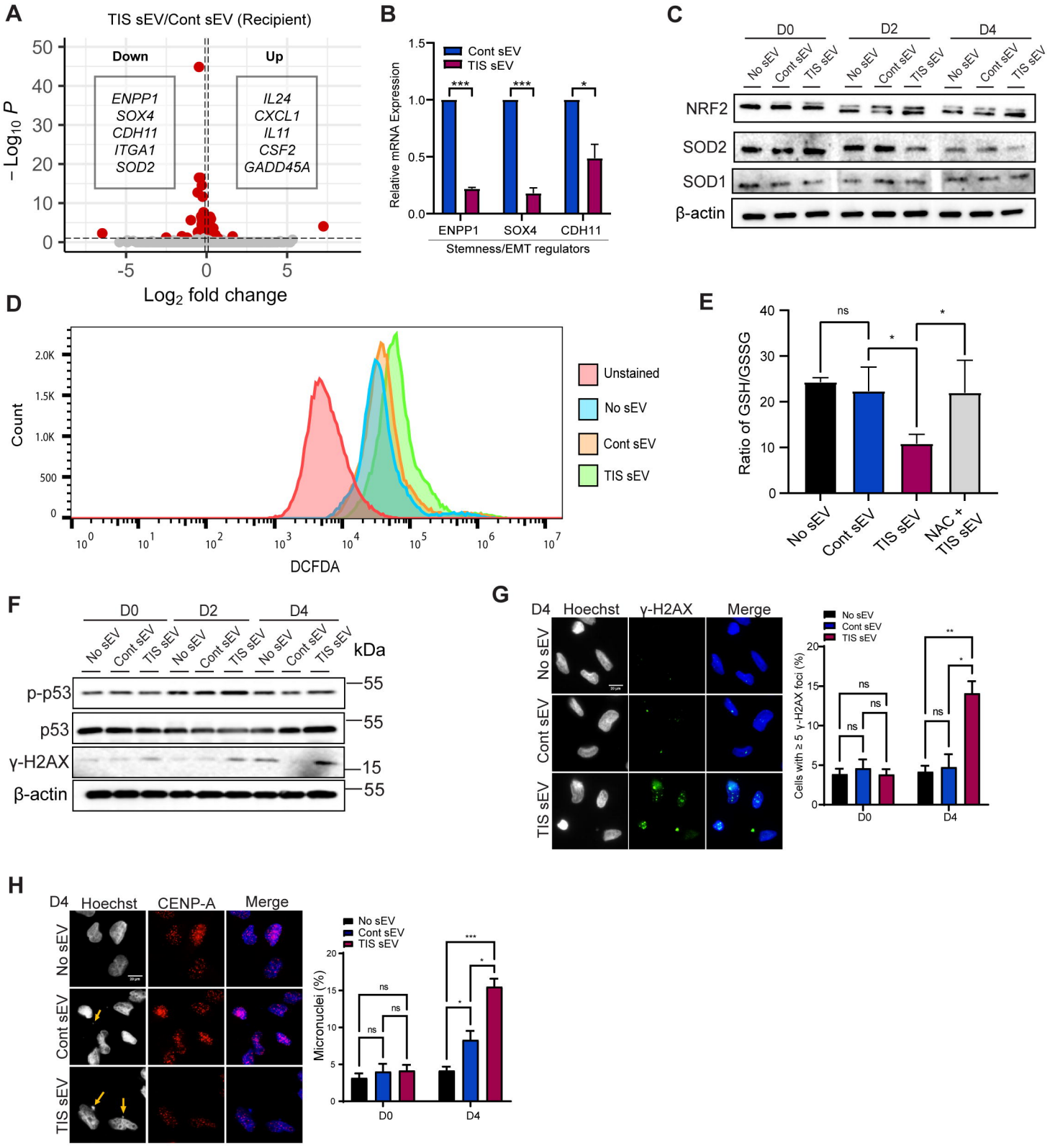

Fig. 4. TIS sEVs induce elevated ROS accompanied by increased DNA damage and micronuclei formation. (A) Volcano plot of differentially expressed genes (DEGs) between MDA-MB-231 incubated with TIS sEV vs Cont sEV. Dashed vertical lines denotes Log2FC ≤ -0.1; Log2FC ≥ 0.1, horizontal lines denotes Padj ≤ 0.1. **(B)** Validation of ENPP1, SOX4, and CDH11 expression by qPCR in cells incubated with sEVs. **(C)** Assesment of ROS-associated proteins NRF2, SOD2, and SOD1 in cells incubated with No sEV, Cont sEVs, and TIS sEVs at day 0 (D0; pre-incubation), day 2 (D2), and day 4 (D4) by Western blotting. **(D)** Flow cytometry analysis of cells stained with DCFDA after 2 days incubation with sEVs. **(E)** Measurement of GSH/GSSG ratio in cells after 2 days incubation with sEVs in the presence or absence of 24h NAC (5mM) pre-treatment. **(F)** Assessment of DNA damage associated proteins p-p53, p53, and γ-H2AX in cells incubated with sEVs at day 0 (D0; pre-incubation), day 2 (D2), and day 4 (D4) by western blot. **(G)** Representative immunofluorescence images and quantification of γ-H2AX positive MDA-MB-231 cells after incubation with sEVs at day 4 (D4). Scale bar: 20 μm. **(H)** Immunofluorescence staining of centromere protein A (CENP-A) and quantification of acentric micronuclei in MDA-MB-231 cells after incubation with sEVs at day 4 (D4). Scale bar: 20 μm.*p < 0.05, **p < 0.01, ***p < 0.001, and n.s. non significance by Student's t-test.